doi:10.1006/jmbi.2000.4419 available online at http://www.idealibrary.com on IDEAL® *J. Mol. Biol.* (2001) **306**, 1023–1035

JMB

Structure of a Eukaryotic Decoding Region A-site RNA

Stephen R. Lynch and Joseph D. Puglisi*

Department of Structural Biology, Stanford University School of Medicine, Stanford CA 94305-5126, USA

**Corresponding author*

The aminoglycoside antibiotics target a region of highly conserved nucleotides in the aminoacyl-tRNA site (A site) of 16 S RNA on the 30 S subunit. The structures of a prokaryotic decoding region A-site oligonucleotide free in solution and bound to the aminoglycosides paromomycin and gentamicin C1A have been determined. Here, the structure of a eukaryotic decoding region A-site oligonucleotide has been determined using homonuclear and heteronuclear NMR spectroscopy, and compared to the unbound prokaryotic rRNA structure. The two structures are similar, with a U1406-U1495 base-pair, a C1407-G1494 Watson-Crick base-pair, and a G1408-A1493 base-pair instead of the A1408-A1493 base-pair of the prokaryotic structure. The two structures differ in the orientation of the 1408 position with respect to A1493; G1408 is rotated toward the major groove, which is the binding pocket for aminoglycosides. The structures also differ in the stacking geometry of G1494 on A1493, which could have slight long-range conformational effects.

Keywords: decoding; structure; oligonucleotide; NMR; eukaryotic 16 S rRNA

Introduction

Decoding is the process in which the ribosome recognizes the correct interaction of the mRNA codon and the cognate tRNA. This interaction occurs at the decoding region aminoacyl-tRNA site (A site) on the small (30 S) ribosomal subunit near the 3′ end of 16 S rRNA in a region of highly conserved nucleotides (Figure 1) (Noller, 1991). The decoding region A site (decoding site) probably contacts the codon-anticodon interaction to ensure accuracy during translation; consistent with this hypothesis, tRNA protects A1492 and A1493 from chemical probes (Moazed & Noller, 1986) and the activity of the deleterious mutations A1492G and A1493G can be recovered *in vitro* by replacing the mRNA with a 2′ fluoro-mRNA (Yoshizawa *et al*., 1999).

The three-dimensional X-ray crystal structures of the 70 S ribosome (Cate *et al*., 1999) and the 30 S (Clemons *et al*., 1999) subunit have confirmed that the penultimate stem of the 30 S subunit, a few base-pairs below the decoding site, contacts the 900 region. Although little of the electron density had been fit in the 70 S structure, the long penultimate stem and the 900 region were identified and shown to be making an RNA-RNA contact, which agrees with the findings from the structure of the 30 S subunit. The proximity of the decoding site to the 900 region is not surprising, considering that the 900 region, containing the switch helix, is critical for fidelity of translation (Lodmell & Dahlberg, 1997). In the 30 S crystal structure, the penultimate stem is in a different conformation and oriented differently with respect to the 900 region, but the two regions of RNA still make the long-range RNA-RNA interaction. The difference in the conformation of the penultimate stem in the two structures suggests that the penultimate stem changes conformation during the translation cycle. Since the penultimate stem contacts other regions of 16 S RNA and is at the subunit interface, a local conformational difference in the decoding site could be transmitted to other regions of the ribosome.

The mechanism of translation of mRNA to protein is conserved in eukaryotes, although it is more complicated than that of prokaryotes. Many regions of rRNA, particularly those involved with important steps of translation, are conserved throughout all organisms. In the decoding site, six of the seven nucleotides in the internal loop are universally conserved, all except for position 1408, which is adenosine in all prokaryotic and mitochondrial 16 S RNA sequences and guanosine in all eukaryotic cytosolic sequences (Gutell, 1994). Higher eukaryotes often have a mispair at positions 1409-1491, but many lower eukaryotes including *Giardia muris* and *Tetrahymena thermophila*

E-mail address of the corresponding author: puglisi@stanford.edu

0022-2836/01/051023–13 $35.00/0

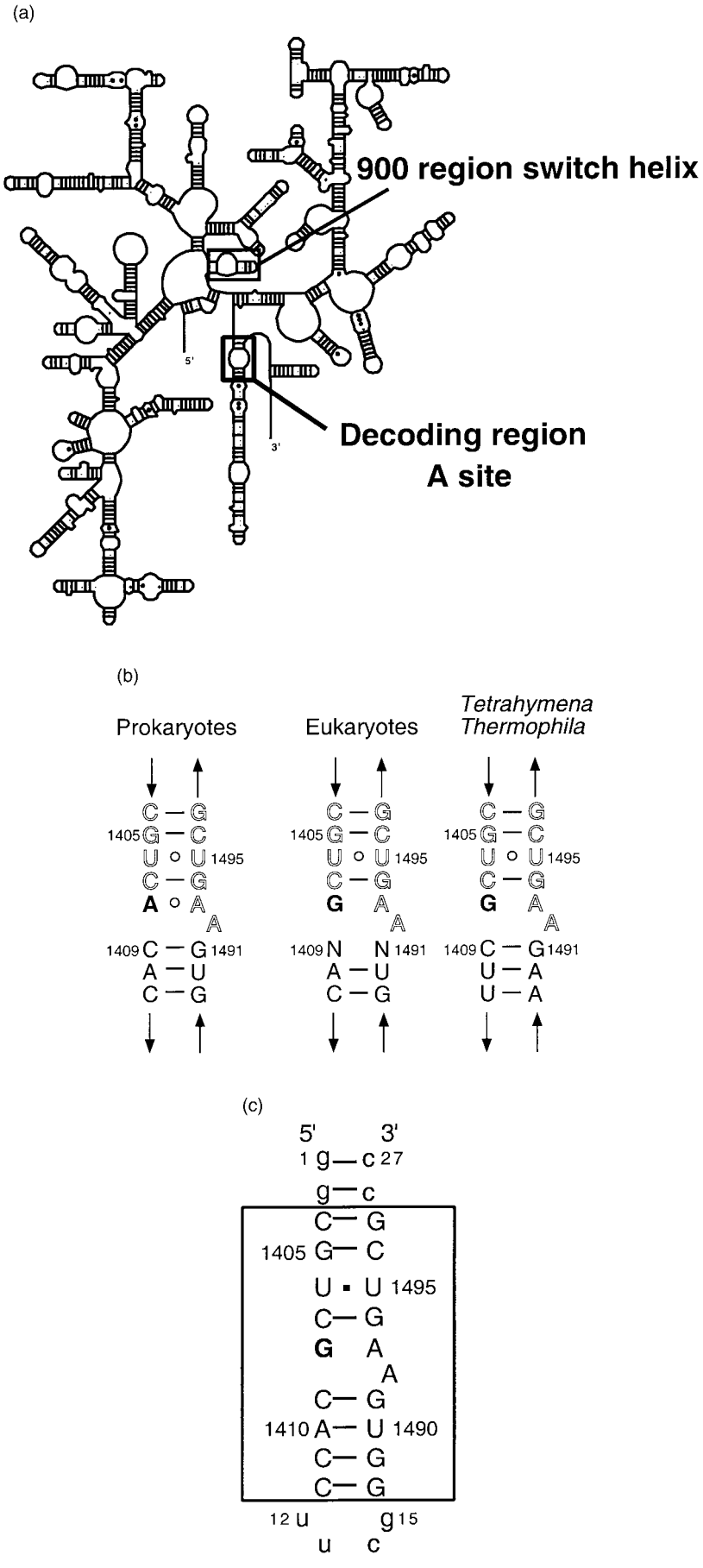

Figure 1. (a) The secondary structure of 16 S rRNA with the decoding region A site and 900 regions highlighted with a box. (b) An enlargement of the boxed region of the decoding site from (a), the consensus secondary structure of the decoding site for prokaryotes, eukaryotes, and *Tetrahymena thermophila*. The nucleotides outlined are universally conserved. Position 1408, an adenosine residue in all prokaryotic sequences and a guanosine residue in all eukaryotic sequences, is highlighted in bold. (c) The eukaryotic decoding region A-site oligonucleotide used in this study with position G1408; the prokaryotic oligonucleotide studied previously is identical except for position A1408 (Recht *et al.*, 1996; Fourmy *et al.*, 1998).

have the C1409-G1491 base-pair (Gutell, 1994). Although these organisms reverse the base-pair below (U1410-A1490 rather than A1410-U1490), this mutation is unlikely to affect the local structure of the asymmetric internal loop (U1406-G1408, A1492-U1495).

Aminoglycoside antibiotics bind to the decoding site of 16 S rRNA (Figure 1) (Moazed & Noller, 1987; Woodcock *et al*., 1991), inducing codon misreading and inhibiting translocation (Davies *et al*., 1965; Edelmann & Gallant, 1977). Despite the high level of phylogenetic conservation of their rRNA target, aminoglycosides specifically target prokaryotic and mitochondrial ribosomes over eukaryotic ribosomes. Since the only sequence difference in the internal loop is at position 1408, this position was expected to be critical in drug binding. In fact, expression of *Escherichia coli* with the mutation A1408G is enough to confer resistance to many aminoglycosides (Recht *et al*., 1999).

NMR structural studies on a model oligonucleotide (Figure 1) of the wild-type *E. coli* sequence free in solution (Fourmy *et al*., 1998), bound to paromomycin (Fourmy *et al*., 1996), and bound to gentamicin C1A (Yoshizawa *et al*., 1998) have shown that three base-pairs are formed in the internal loop (Figure 1), including a U1406-U1495 pair and an A1408-A1493 pair. The geometry of the A1408-A1493 pair observed in the three oligonucleotide structures cannot be isosterically duplicated by a G1408-A1493 pair, which occurs in the eukaryotic sequence (Figure 2). This study is aimed at determining the structure of an oligonucleotide that mimics the eukaryotic decoding region A site (Figure 1). The structures were determined with homonuclear and heteronuclear NMR experiments, and compared to the previous wild-type structures. The structure shows a slight conformational difference in the eukaryotic decoding site in comparison with the prokaryotic decoding site that could be important in the resistance to aminoglycosides and to long-range conformational effects during translation.

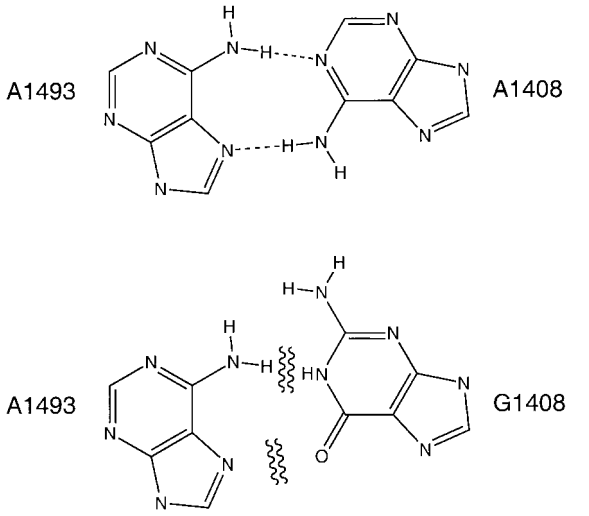

Figure 2. The geometry of the A1408-A1493 base-pair identified previously; the amino proton of A1408 hydrogen bonds to N7 of A1493, and the amino proton of A1493 hydrogen bonds to N1 of A1408. This base-pair cannot be replaced by the same base-pair with G1408-A1493, since N1 of guanosine is a hydrogen bond donor and O6 is a hydrogen bond acceptor.

Results

Oligonucleotide design

The secondary structure of the decoding site of 16 S RNA is highlighted in Figure 1, including the universally conserved U1406-U1495 base-pair, the C1407-G1494 base-pair, A1492 and the 1408 purine-A1493 pair. The eukaryotic oligonucleotide studied is the 27 nucleotide RNA presented in Figure 1(c) with G at position 1408 rather than A as in the prokaryotic sequence. The oligonucleotide was designed to mimic a minimal eukaryotic decoding site to compare to the structure of the prokaryotic decoding site previously determined. Prior data have demonstrated the validity of this oligonucleotide system for study of the local structure of rRNA in the decoding site (Recht *et al*., 1996).

Comparison of the thermodynamics of eukaryotic and prokaryotic decoding-site oligonucleotides

The thermodynamics of the eukaryotic and prokaryotic oligonucleotides was studied by UV absorbance melting curves. Multiple melts at similar concentrations (1.5 μM) were measured and averaged for both oligonucleotides, and the results are presented in Table 1. The melting temperature measured for the prokaryotic decoding-site oligonucleotide is 68.2(±0.4) °C in comparison to 69.9(±0.5) °C for the eukaryotic oligonucleotide. The 2 deg. C higher melting temperature indicates slightly greater thermodynamic stability for the eukaryotic oligonucleotide.

Table 1. Thermodynamic parameters for eukaryotic and prokaryotic oligonucleotides

	T_M (°C)	$\Delta G°$ (37 °C) (kcal/mol)	$\Delta H°$ (kcal/mol)	$\Delta S°$ (kcal/mol K)
Eukaryotic	69.9 ± 0.5	−6.4 ± 0.2	−70.3 ± 2.1	−0.21 ± 0.01
Prokaryotic	68.2 ± 0.4	−5.7 ± 0.2	−63.6 ± 2.4	−0.18 ± 0.07

NMR assignments of the free form of the eukaryotic decoding-site oligonucleotide

The quality of the NMR spectra of the eukaryotic decoding-site oligonucleotide was good; a $^{13}C/^{1}H$-HSQC is shown in Figure 3. Two regions of the spectrum are presented: the upfield aromatic region with most of the guanosine H8-C8 resonances and the downfield aromatic region with the adenosine C2-H2 resonances. These resonances are sharp and well dispersed when spread over two dimensions, which is important for dispersion of NOEs in a 3D $^{13}C/^{1}H/^{1}H$ HSQC-NOESY. Included in these regions of the spectrum are some of the resonances most likely affected by position G1408 of the eukaryotic oligonucleotide in comparison with the prokaryotic oligonucleotide previously studied (Fourmy *et al*., 1998).

A more detailed comparison of assignments of the two free-form oligonucleotides is shown in Table 2 for the base and H1′ protons for the core nucleotides (G1405-A1410, U1490-C1496). Chemical shift is a very sensitive indicator of change in local chemical environment surrounding a proton. Differences are observed at A/G 1408, C1409, and the other side of the helix G1491-G1494. The differences in chemical shift at nucleotide 1408 are not necessarily significant, because guanosine in solution has different chemical shifts than adenosine. The chemical shift differences on the other side of the helix probably result from conformational differences between the prokaryotic and eukaryotic oligonucleotide conformations.

NMR characteristics of the eukaryotic decoding-site oligonucleotide

All non-exchangeable protons and most exchangeable protons were assigned for the eukaryotic decoding-site oligonucleotide with homonuclear and heteronuclear (^{13}C, ^{15}N, ^{31}P) 2D, 3D, and 4D experiments. The expected NOEs for *A*-form RNA, including those from the H1′, H2′, and H3′ protons to the intranucleotide H8/6 protons and the H8/6 protons of the sequential nucleotide, were observed from g1 through C1412 including the C1407 to G1408 and G1408 to C1409 steps. H1′/H2′ crosspeaks were detected in the $^{1}H/^{1}H$-DQF-COSY or short mixing time (20 ms) $^{1}H/^{1}H$-TOCSY for C1409 and g1, which is typically dynamic. The DQF-COSY H1′-H2′ crosspeak for C1409 was very weak, indicating a conformational equilibrium that favors a C3′-*endo* sugar pucker. The imino proton for G1408 was never assigned, although a very weak NOE was observed between the G1491 imino resonance and an imino resonance at the same chemical shift as that of G1489. Although G1491 and G1489 are two base-pairs apart and thus too far for a real NOE, a crosspeak between the two resonances could result from spin diffusion. Crosspeaks between imino protons two base-pairs apart were not observed for any of the other imino resonances, but spin diffusion cannot be discounted. The potential G1408 imino resonance could not be resolved from that of G1489 at different temperature or different pH in a 1D or 2D $^{1}H/^{15}N$ HSQC. The linewidths of the H8 and C8 resonances for G1408 were broader than those of the stem residues, and thus the intensity of the H8-C8 peak in the $^{13}C/^{1}H$ HSQC was weaker than those of the stem residues. Additionally, the intranucleotide sugar-sugar NOEs of G1408 (H1′-H2′, H1′-H3′, H1′-H4′) were weaker than for other residues. These results suggest line-broadening of the G1408 resonances, including the imino proton, resulting from intermediate exchange dynamics.

The UUCG tetraloop has unusual NMR characteristics that have been described elsewhere

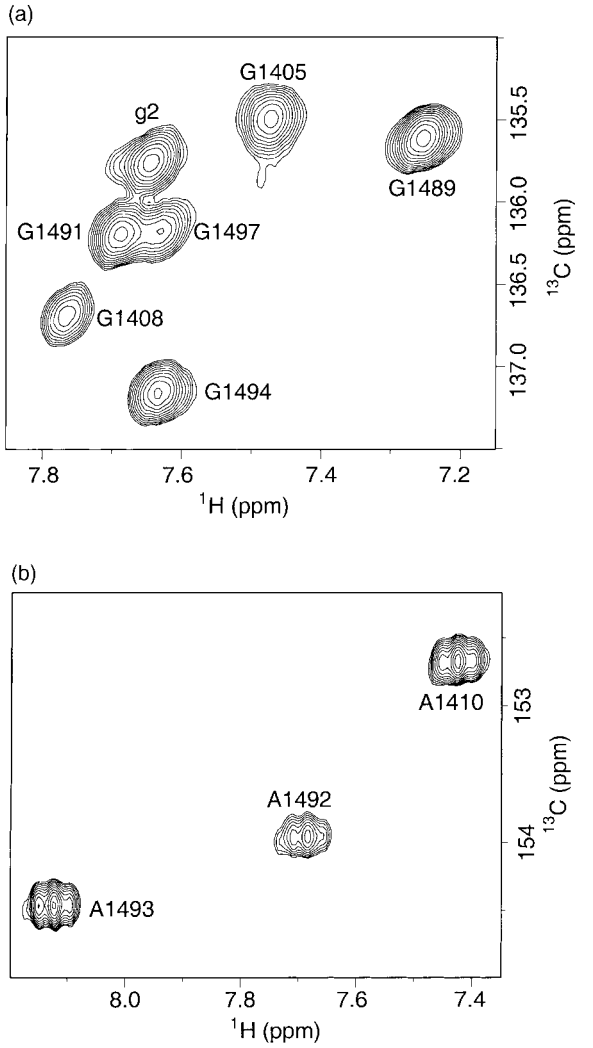

Figure 3. (a) The guanosine C8-H8 portion of a 2D $^{13}C/^{1}H$ HSQC acquired on the eukaryotic decoding-site oligonucleotide shown in Figure 1(c) is presented. The RNA was dissolved in 10 mM sodium phosphate buffer (pH 6.3), 10 μM EDTA. The spectrum was acquired with 16 scans of 2048 complex points in ω2 by 256 in ω1 on a 500 MHz Varian Inova spectrometer at 25 °C. (b) The adenosine H2-C2 portion of the same HSQC.

Table 2. Comparison of NMR chemical shifts of prokaryotic and eukaryotic oligonucleotides

>	H8/6		H5/2		H1′		Imino	
	G1408	A1408	G1408	A1408	G1408	A1408	G1408	A1408
G1405	7.47	7.47	-	-	5.74	5.74	13.30	13.30
U1406	7.58	7.57	5.22	5.20	5.47	5.45	10.71	10.65
C1407	7.99	7.99	5.74	5.73	5.74	5.69	-	-
A/G1408	**7.77**	**8.14**	-	7.86	**5.83**	**6.01**	nm	-
C1409	**7.65**	**7.54**	5.43	5.38	**5.46**	**5.26**	-	-
A1410	8.19	8.16	7.43	7.48	5.87	5.84	-	-
U1490	7.64	7.65	5.17	5.17	5.56	5.56	13.97	13.98
G1491	7.70	7.68	-	-	5.66	5.70	**12.23**	**12.35**
A1492	8.12	8.11	**7.68**	**7.95**	5.98	5.92	-	-
A1493	8.37	8.30	8.11	8.11	6.09	6.03	-	-
G1494	**7.62**	**7.42**	-	-	**5.66**	**5.55**	**13.14**	**12.78**
U1495	7.62	7.60	5.20	5.16	5.52	5.47	10.22	10.25
C1496	8.06	8.04	5.85	5.82	5.75	5.73	-	-

[1]H chemical shift was measured at 25 °C for non-exchangeable protons; 5 °C for exchangeable protons. The sample was ~3 mM RNA in 10 mM sodium phosphate (pH 6.3).

Resonances that differ by >0.1 ppm are indicated in bold; nm, not measured.

(Cheong *et al*., 1990; Varani *et al*., 1991; Varani & Tinoco, 1991). G1491 and G1494 had very weak H1′/H2′ crosspeaks in the DQF-COSY and short mixing time (20 ms) TOCSY indicates either dynamics of the sugar pucker for those nucleotides or a sugar pucker other than C3′-*endo* or C2′-*endo*. Additionally, the 3′-terminal cytidine residue (c27) had a moderate H1′/H2′ crosspeak in a short mixing time TOCSY and DQF-COSY, consistent with dynamics at the end of the helix. The NOEs expected in *A*-form helices were observed for all nucleotides from G1488-c27, except for G1491-A1492, A1492-A1493, and A1493-G1494. The two adenosine residues of the internal loop had a number of unusual NOEs, including both A1492 H2 and A1493 H2 to C1409 H1′, A1492 H2-A1493 H2 and H8. Additionally, both A1492 and A1493 had strong H1′/H2′ crosspeaks in a DQF-COSY and short mixing time TOCSY indicating C2′-*endo* sugar puckers for both nucleotides.

Structure of eukaryotic decoding-site oligonucleotide free in solution

The structure for the eukaryotic decoding-site oligonucleotide was calculated from 682 NOEs, 129 experimentally determined dihedral constraints, and 36 hydrogen bonds for the Watson-Crick base-pairs; structure statistics are presented in Table 3. A total of 100 structures were calculated, of which 31 converged to low energy after the global fold; the NOE and dihedral violation energies for six structures were high after refinement with torsion angle restraints and were discounted. A superposition of the 25 lowest-energy structures of the eukaryotic oligonucleotide is presented in Figure 4(a). The overall heavy-atom r.m.s.d. for the RNA is 1.50 Å. In comparison, the heavy-atom r.m.s.d. for the free form of the prokaryotic decoding-site oligonucleotide was 1.10 Å. Excluding the 1408 position, the r.m.s.d. for the eukaryotic oligonucleotide is 1.47 Å, and 0.95 Å for the prokaryotic oligonucleotide.

One of the main reasons for the disorder of the eukaryotic oligonucleotide structure is the lack of long-range constraints, which allow for a variety of bend angles through the long helix; another possible reason for disorder is dynamics, particularly within the internal loop or from the internal loop to the two helical stems. The superposition of 25 structures of the core nucleotides G1405-A1410, U1490-C1496 is presented in Figure 4(b); the r.m.s.d. for these nucleotides is 0.85 Å and 0.80 Å for the core residues without position 1408. In comparison, the r.m.s.d. for the core residues for the

Table 3. Structure statistics and atomic r.m.s. deviations

Distance constraints	
Total	682
Internucleotide	427
Internal loop	203
Internucleotide internal loop	132
Dihedral constraints	129
Hydrogen bonds (WC base-pairs)	36
Final forcing energies (kcal/mol)	
Distance and Dihedral constraints	11.7 ± 3.2
r.m.s.d from distance constraints (Å)	
All (682)	0.014
r.m.s.d. from experimental dihedral	
Constraints (deg.) (129)	0.882
Deviations from idealized geometry	
Bonds (Å)	0.108
Angles (deg.)	6.76
Impropers (deg.)	0.222
Heavy-atom r.m.s.d	
All RNA	1.50 ± 0.42
Core residues	0.84 ± 0.30

Final minimized structures are compared to the average coordinates of the 25 final structures best-fitted to each other. The final structures did not contain any NOE violations > 0.2 Å or torsion angle violations > 10 °. Core residues refer to G1405-A1410 and U1490-C1496. Internal loop residues refer to U1406-G1408 and A1492-U1495. WC base-pairs are Watson-Crick G-C and A-U base-pairs.

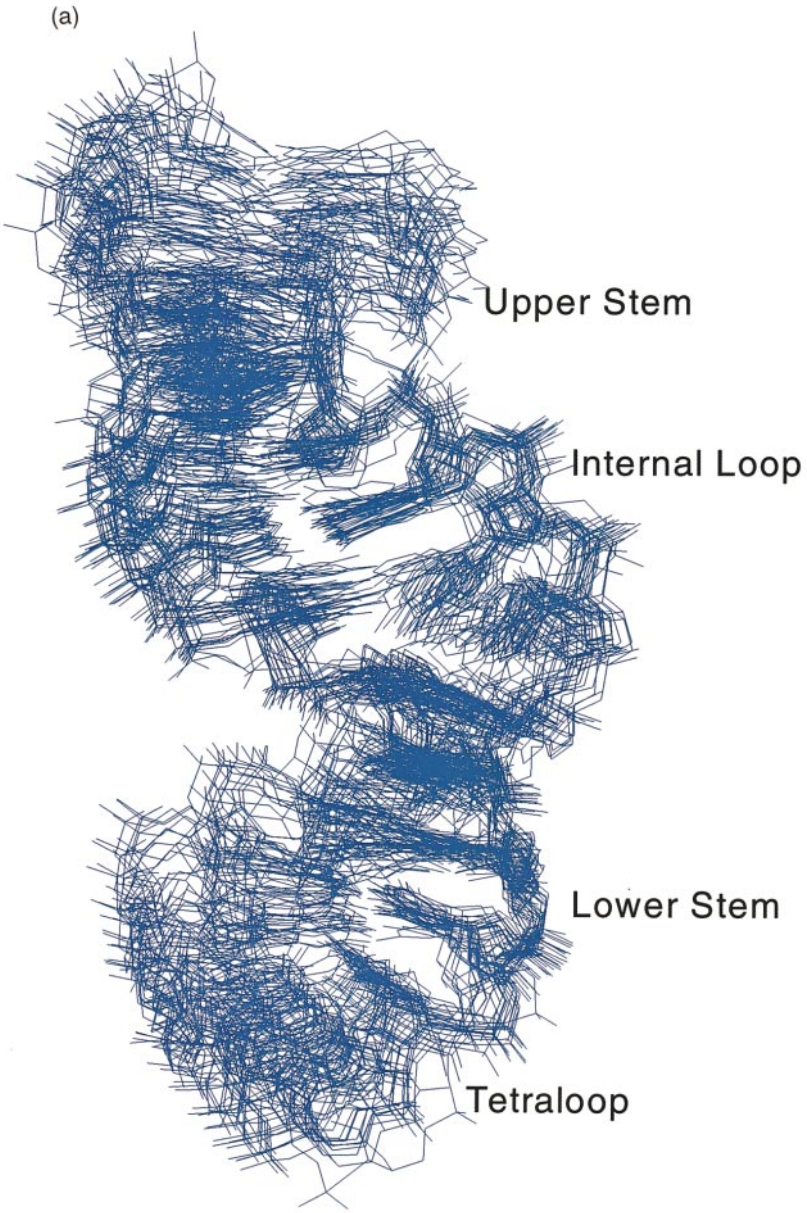

Figure 4(a) (*legend opposite*)

prokaryotic structure was 0.93 Å and 0.95 Å for the core residues without the 1408 position.

A comparison of the minimized average structures for the free form of the prokaryotic and eukaryotic decoding-site oligonucleotides is presented in Figure 5. The global structures of the two oligonucleotides are similar; the upper stem, lower stem, and UUCG tetraloop are basically equivalent. The overall r.m.s.d. of the single structures of the prokaryotic and eukaryotic decoding-site oligonucleotides is 3.87 Å. The internal loops are similar, in that U1406 base-pairs to U1495, C1407 base-pairs to G1494, and the 1408 position interacts with A1493. The r.m.s.d. of the single structures of the prokaryotic and eukaryotic decoding-site oligonucleotides of only the internal loop residues is 3.56 Å. The geometry of the U-U pair for the 25 structures of the eukaryotic oligonucleotide is shown in Figure 6. The r.m.s.d. to the average structure for the bases of U1406 and U1495 is 0.27 Å; in comparison, the r.m.s.d. for the same bases in the prokaryotic structures is 0.07 Å. In the structures, U1495 N3 forms a hydrogen bond to U1406 O2 (3.53(±0.55) Å), and U1406 N3 forms a hydrogen bond to U1495 O4 (3.48(±0.66) Å). The alternative pairing geometry for a U-U base-pair is disfavored in the structure; the distance from U1406 N3 to U1495 O2 is 6.21(±0.21) Å, and from U1406 04 to U1495 N3 it is 6.18(±0.25) Å. The U-U pair in the prokaryotic sequence favors the same geometry, but the difference between the two possible hydrogen bonding schemes is not as dramatic,

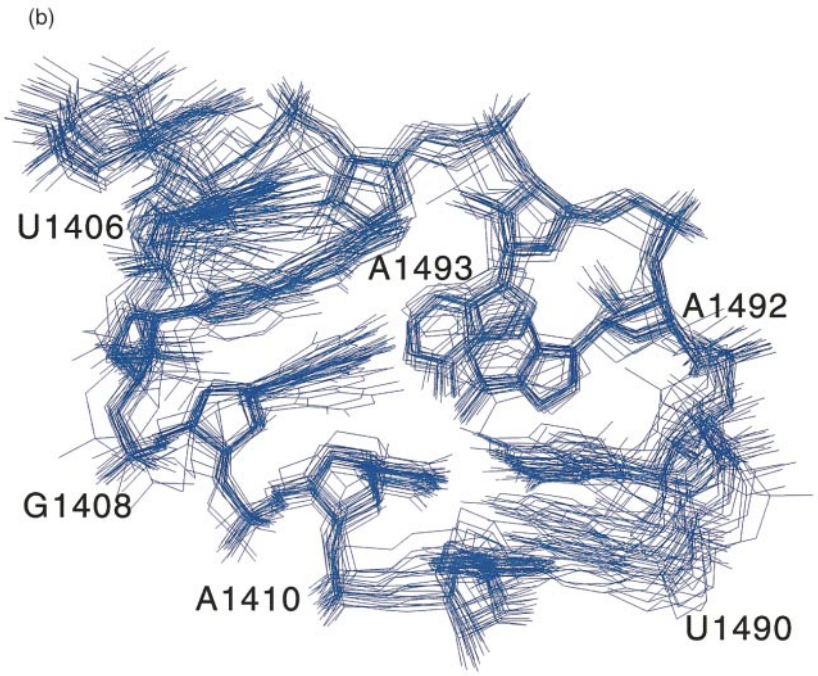

Figure 4. (a) Superposition of the 25 lowest-energy structures of the eukaryotic decoding-site oligonucleotide presented in Figure 1(c); the r.m.s.d of these structures to the average was 1.50 Å. (b) Superposition of the 25 lowest-energy structures of the core residues (G1405-A1410, U1490-C1496) of the eukaryotic decoding-site oligonucleotide; the r.m.s.d. of these structures to the average was 0.85 Å.

although the hydrogen bond donors and acceptors are closer together. In the prokaryotic oligonucleotide, the distance from U1406 N3 to U1495 O4 is 3.44(±0.24) Å, from U1406 N3 to U1495 O2 it is 4.90(±0.20) Å; the distance from U1495 N3 to U1406 O2 is 4.26(±0.23) Å, from U1495 N3 to U1406 O4 it is 4.29(±0.20) Å.

In this study, U1406 and U1495 imino protons could be assigned using through-bond experiments (Simorre *et al*., 1995), which correlate the imino NH and base H6 resonances. In the study of the prokaryotic sequence, the imino resonances for U1406 and U1495 could not be assigned from each other. By unambiguously assigning both imino resonances using through-bond correlation experiments, the stronger NOE from the U1406 imino to U1495 H5 than the U1495 imino to the U1406 H5 can be confidently distinguished, confirming the observed geometry.

The G1408-A1493 base-pair is not well defined in the structure; the r.m.s.d. of the bases for G1408 and A1493 in the low-energy structures is 0.45(±0.40) Å. Likewise, the A1408-A1493 base-pair is not well defined in the prokaryotic sequence free form, the r.m.s.d for the bases of A1408 and A1493 is 0.47(±0.34) Å. In the eukaryotic oligonucleotide, only one amino proton was observed for A1492 and A1493, and exchangeable proton resonances for G1408 were not assigned. A moderate A1493 (H2)-C1409 (H1′) NOE places the Watson-Crick face of A1493 toward G1408; C1407 ribose to G1408 H8 NOEs, G1408 ribose to C1409 H5 and H6, and a G1494 imino proton to G1408 H1′ NOEs position the Watson-Crick face of G1408 toward A1493. The range of low-energy structures (Figure 7) suggests a single hydrogen bond from the G1408 amino group to A1493 N1 (2.90(±0.21) Å), but the base-pair is probably dynamic or involves water-mediated hydrogen bonds.

G·A base-pairs are observed in many RNA structures, with two base-pairing geometries: the sheared G·A, in which the adenosine amino group hydrogen bonds to the guanosine N3 and the guanosine amino group hydrogen bonds to the adenosine N7, and the normal G·A imino base-pair, in which the guanosine imino group hydrogen bonds to the adenosine N1 and the adenosine amino group hydrogen bonds to the guanosine O6. If the G1408-A1493 base-pair was a sheared G·A, several NOEs that are not observed, including C1407 H5-G1408 H8, would be observed. Additionally, several NOEs observed, including the strong intensity C1407 H2′-G1408 H8, should have intensities that differ significantly from what was observed. The normal G·A imino base-pair would have *A*-form like NOEs, and thus cannot be discounted from the NMR data. Although, as a whole, the structures show that the N1 of G1408 is 4.80(±0.70) Å from the N1 of A1493, G1408 N1 and A1493 N1 in two of the low-energy structures are only 2.7 Å apart.

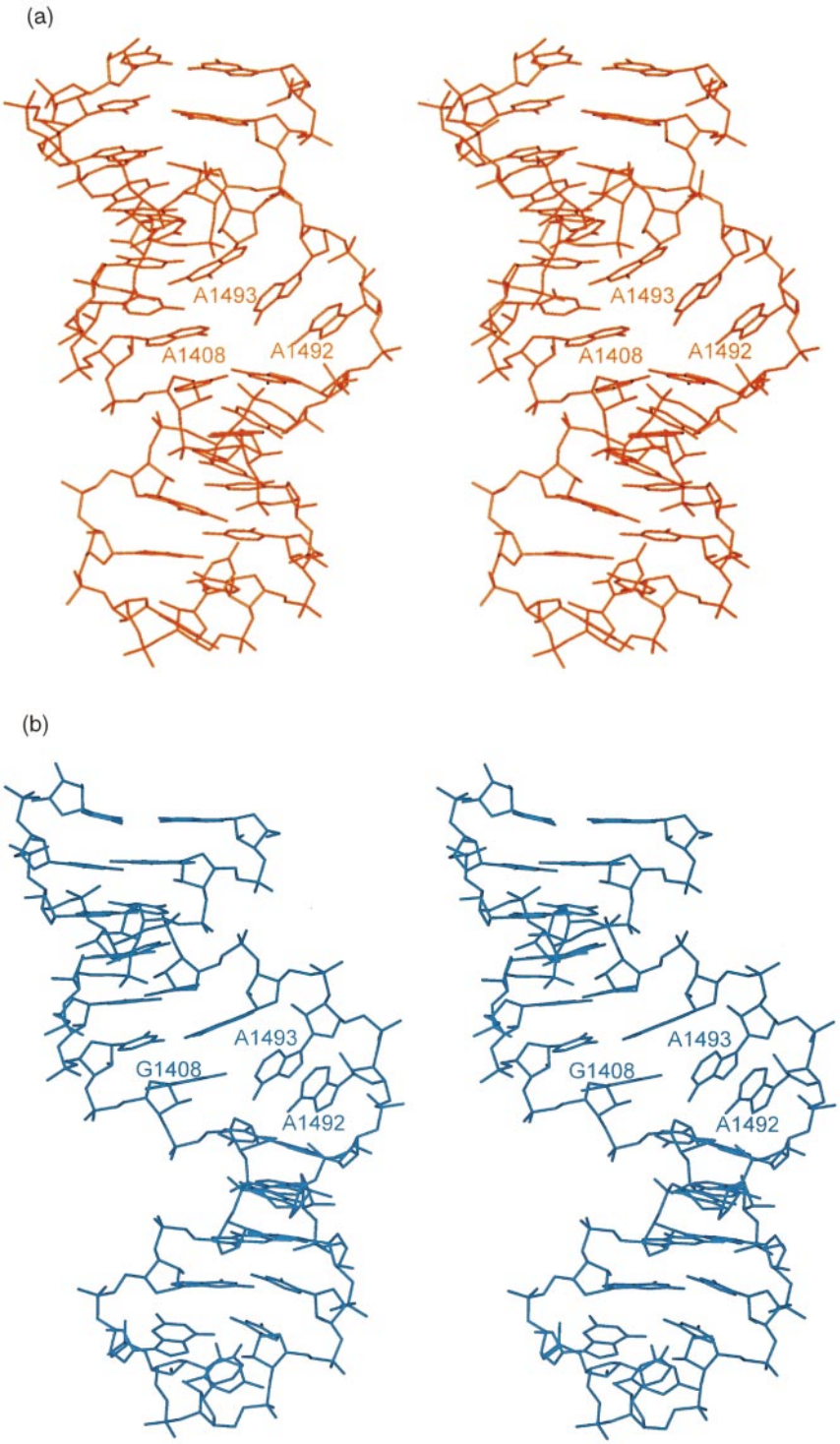

Figure 5. A comparison of the minimized average structures (stereo) of the eukaryotic decoding-site oligonucleotide (blue) and the prokaryotic decoding-site oligonucleotide (red). The structure of the prokaryotic sequence was determined previously (Fourmy *et al.*, 1998).

Differences between the structures of the prokaryotic and eukaryotic decoding-site oligonucleotides

The structure of the lower stem nucleotides (C1409-C1411, G1489-G1491) of the eukaryotic decoding A-site oligonucleotide was superimposed on that of the prokaryotic decoding-site oligonucleotide (Figure 8). The position of the internal loop nucleotides relative to the lower stem for the two structures is quite different. A1492 and A1493 are much closer to C1409 in the eukaryotic oligonucleotide structure than in the prokaryotic oligonucleotide structure. In the prokaryotic oligonucleotide structure, the N7 and N1 positions on A1492 are 8.03 Å and 8.56 Å, respectively, from N3 of C1409; the same positions are 4.0 Å and 5.59 Å in the eukaryotic structure. Similarly, the

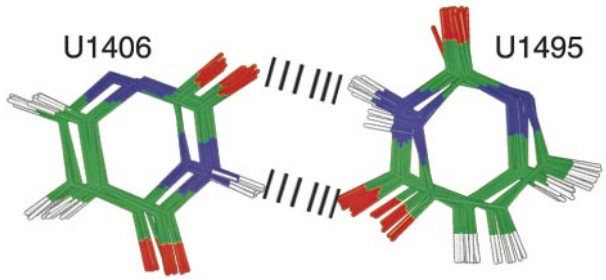

Figure 6. A superposition of the base-pair formed between U1406 and U1495. The atoms are shown by their defined atomic color (carbon, green; oxygen, red; nitrogen, blue; hydrogen, gray). Hydrogen bonds are indicated by a broken line.

N7 and N1 positions of A1493 are further from C1409 in the prokaryotic RNA (8.06 Å and 5.81 Å in the prokaryotic RNA *versus* 5.4 Å and 4.25 Å in the eukaryotic RNA). A1492 and A1493 both have NOEs to C1409 H1′, which forces the two bases closer to C1409 than in the prokaryotic structure. Additionally, G1408 is shifted approximately 1.5 Å in comparison to A1408 relative to C1409; the distance from A1408 N3 to C1409 C6 is 4.8 Å *versus* 5.5 Å for G1408-C1409, and A1408 N7 to C1409 C6 is 4.3 Å *versus* 6.6 Å for G1408-C1409. This structural difference is consistent with additional NMR information. For example, the chemical shifts of C1409 protons are greatly affected by the nucleotide at position 1408. Particularly, the H1′ is shifted upfield in the prokaryotic oligonucleotide, and in the structure, A1408 is shifted toward the other side of the helix relative to C1409.

A1492 and A1493 are oriented similarly in the two structures but are displaced relative to C1409 (Figure 8). The adenosine residues of the two structures superimpose well, showing that they are in

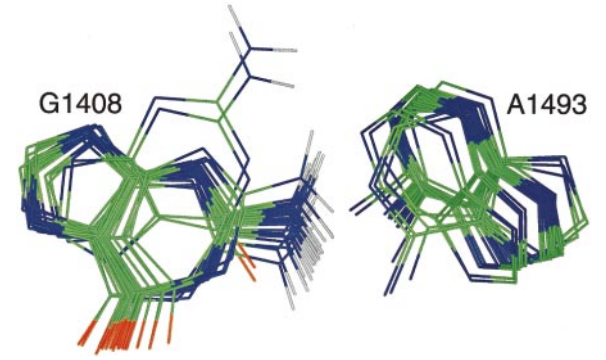

Figure 7. A superposition of the bases of G1408 and A1493. The atoms are shown by their defined atomic color (carbon, green; oxygen, red; nitrogen, blue; hydrogen, gray). The only hydrogen atoms shown are the amino protons of G1408. The structures suggest a single hydrogen bond from the amino protons of G1408 to A1493 N1.

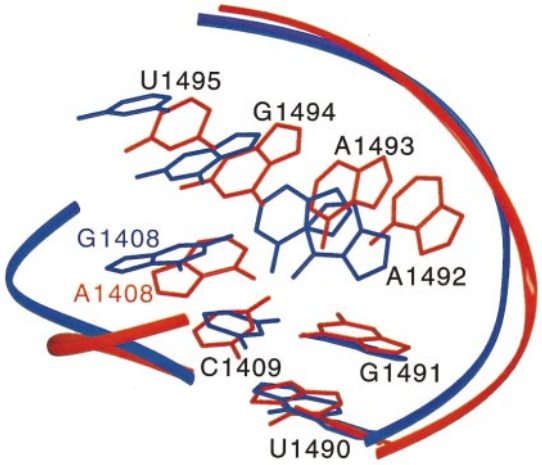

Figure 8. The lower stem residues (C1409-C1411; G1489-G1491) of the minimized average structure of the eukaryotic decoding-site oligonucleotide (blue) were superimposed on the same nucleotides of the minimized average structure of the prokaryotic decoding-site oligonucleotide (red). The ribbons represent the phosphodiester backbone. This Figure highlights the difference in position of the internal loop relative to the lower stem.

the same conformation relative to each other, but the base at 1408 is oriented differently with respect to the adenosine residues (Figure 9). G1408 is rotated towards the major groove relative to A1408. The O6 position points into the major groove. Thus, the shape of the major groove is altered in the eukaryotic oligonucleotide.

The change in the position of G1408 with respect to A1492 and A1493 changes the stacking geometry of A1493 on G1494 (Figure 10). Chemical shift data (Table 2) suggested that the base of G1494 was affected by the different nucleotide at position 1408: a 0.2 ppm downfield shift of H8 and a 0.36 ppm upfield shift of the imino proton were observed for the eukaryotic RNA relative to the prokaryotic RNA. Presumably, the steric bulk of the guanosine 2-amino group compared to the H2 proton of the adenosine residue displaces A1493 and results indirectly in a difference in stacking of A1493 and G1494.

Discussion

The eukaryotic decoding-site oligonucleotide adopts a global structure similar to that of the prokaryotic decoding-site oligonucleotide. This region of the rRNA in eukaryotes is involved with decoding the mRNA through interaction with A-site bound tRNA and mRNA as in prokaryotes. The conserved nature of mRNA decoding in prokaryotes and eukaryotes suggests conserved rRNA contacts, consistent with the high level of sequence conservation of the decoding region A site. Large perturbations in rRNA structure of the eukaryotic decoding site are not expected, and *E. coli* grown

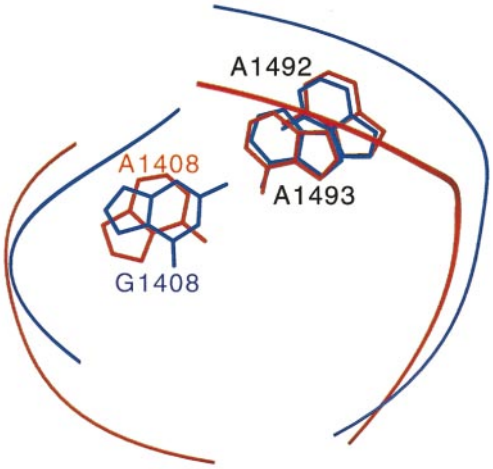

Figure 9. A1492 and A1493 of the eukaryotic decoding-site oligonucleotide (blue) were superimposed on the same nucleotides of the prokaryotic decoding-site oligonucleotide (red). This Figure highlights the difference in orientation of the 1408 position relative to the other side of the helix.

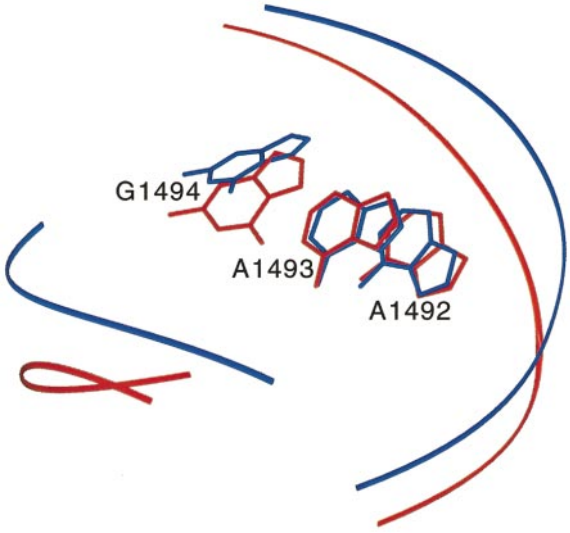

Figure 10. A1492 and A1493 of the eukaryotic decoding-site oligonucleotide (blue) were superimposed on the same nucleotides of the prokaryotic decoding-site oligonucleotide (red). This Figure highlights the difference in orientation of G1494 relative to A1493 and A1492 in the eukaryotic sequence.

with the mutation A1408G are viable, with a growth-rate comparable to that of wild-type (Recht *et al*., 1999). The mutation must not alter the structure of the decoding region enough to prevent binding of mRNA and tRNA, interactions with other regions of the ribosome such as the 900 region, or subunit association. However, the mutation is enough to confer resistance to some antibiotics, consistent with a minor change in RNA structure (Recht *et al*., 1999).

The primary difference in the structures of the eukaryotic and prokaryotic decoding region A-site oligonucleotides is the orientation of the 1408 position relative to A1492 and A1493. The prokaryotic A1408-A1493 base-pair geometry (Figure 2) cannot be replaced by a G1408-A1493 base-pair, and to compensate the G1408 base rotates towards the major groove. A single hydrogen bond is formed in the structure from the guanosine amino group to N1 of A1493, but the base-pair is likely dynamic, which was observed for the A1408-A1493 base-pair (Fourmy *et al*., 1998). The geometry of the G1408-A1493 base-pair places the guanosine carbonyl O6 in the major groove. Aminoglycoside antibiotics bind in the major groove (Fourmy *et al*., 1996), and the binding pocket for ring I of the aminoglycoside is created by the A1408-A1493 base-pair (Fourmy *et al*., 1996). The G1408 mutation in *E. coli* confers resistance to aminoglycosides with amino groups at the 6′ position on ring I (Recht *et al*., 1999). The positioning of O6 of G1408 in the major groove would likely interfere with the binding of ring I of the drugs (see the accompanying paper, Lynch & Puglisi, 2001).

The other two differences observed in the structures of the prokaryotic and eukaryotic oligonucleotides are (1) an approximately 2.5 Å difference in the position of A1492, A1493 and the 1408 nucleotide with respect to C1409, and (2) an approximately 20° difference in the orientation of G1494 with respect to A1492 and A1493. Also, A1492 and A1493 change conformation when binding paromomycin (Fourmy *et al*., 1996); the two bases are displaced toward the minor groove and change orientation relative to G1494 and the helical axis. The different orientation of the two adenosine residues in the prokaryotic RNA-paromomycin structure is more dramatic, with an approximately 55° change in orientation of the base of A1492 relative to the helical axis, as opposed to only a 20° difference in the eukaryotic oligonucleotide. Additionally, A1492 and A1493 are displaced toward the minor groove in the prokaryotic RNA-paromomycin complex, which was not observed with the eukaryotic oligonucleotide. NMR structure determination using only scalar coupling constants and NOEs is a good method for analyzing local structural differences such as the stacking of A1493 and G1494, but a poor method of analyzing bending and rise per residue. The structural changes discussed above may be propagated down the helix as a slight change in bending of the helix or a slight change in the helical parameter of nucleotides per turn of helix.

The *E. coli* ribosomal initiation factor 1 (IF1) binds to the decoding region of 16 S rRNA, exhibiting footprints at A1492 and A1493, and an enhancement of reactivity at A1408 (Moazed *et al*., 1995; Dahlquist & Puglisi, 2000). The A1408G mutation eliminated the footprints at A1492 and A1493, as well as all other markers of binding of IF1 to the 30 S subunit (Dahlquist & Puglisi, 2000).

This result suggests that IF1 is not binding to 30 S subunits with position G1408 and, since IF1 is an essential gene and *E. coli* with an A1408G mutation is viable, ribosomes with position 1408G do not require the function of IF1. Although the exact function of IF1 is not known, Dahlquist and Puglisi suggest that IF1 changes the conformation of the 30 S subunit to make it competent for initiation (Dahlquist & Puglisi, 2000). This suggests that the G1408 mutation causes a conformational change in the ribosome to enable initiation in the absence of IF1. This conformational change could result from the local differences propagated down the penultimate stem and possibly to the 900 region, which is known to interact with the penultimate stem in the vicinity of the 1413-1487 base-pair (Cate *et al*., 1999; Clemons *et al*., 1999).

Comparison of the structures of the eukaryotic and prokaryotic decoding region A-site oligonucleotides allows for an analysis of structural similarities critical for proper decoding of the mRNA and differences that lead to aminoglycoside resistance and to differences in translation in lower eukaryotes.

Materials and Methods

NMR sample preparation

Milligram quantities of the decoding region A-site oligonucleotides were prepared unlabeled and uniformly ^{13}C,^{15}N-labeled by *in vitro* transcription from an oligonucleotide template and purified as described (Puglisi & Wyatt, 1995). After electro-elution and precipitation in ethanol, the RNA pellet was resuspended in 10 mM sodium phosphate (pH 6.3), 20 μM EDTA. The sample was then dialyzed against the phosphate buffer with a stepwise decrease in sodium chloride from 1 M to 0 M in a microdialysis apparatus with a 1000 Da cut-off membrane. The buffer used for most NMR experiments was 10 mM sodium phosphate (pH 6.3), 20 μM EDTA. Some H_2O NOESY experiments were acquired in pH 5.75 buffer to slow the exchange rate of imino protons. The RNA concentration was 3 mM for the unlabeled eukaryotic oligonucleotide, and 2.1 mM for the fully ^{13}C,^{15}N-labeled RNA in 225 μl in a Shigemi NMR tube.

UV melting curves

UV melting curves were acquired on a Cary spectrometer with Varian software. The temperature was recorded separately for each of 12 cuvettes, six with RNA samples and six reference cuvettes. The buffer used was 20 mM sodium phosphate (pH 6.5). The samples used were purified in the same way as for NMR spectroscopy. The concentration was approximately 0.15 μM for all samples, which has an absorbance in the 1 cm path-length cuvettes of approximately 0.4. The melts were scanned over the temperature range of 20 °C to 95 °C at a rate of 0.25 deg. C/minute. Thermodynamic parameters were extracted from the data using the Varian ADL (Applications Development Language) software. This software calculates T_M, K (at any temperature), ΔG° (at any temperature), ΔH°, and ΔS° using established methods of calculating thermodynamic parameters from melting curves (Marky & Breslauer, 1987). The program converts the absorbance *versus* temperature plot to a plot of hybridized strands remaining as a function of temperature. A linear least-squares line is calculated between the points in the lower and upper baselines of the absorbance *versus* temperature plot, and extrapolated to the end of the melting curve. If x is the distance from the curve to the upper line and y is the distance from the curve to the lower line, then:

$$\alpha(T) = x/(x + y)$$

where α is the fraction of duplex at a give temperature. If α is plotted *versus* temperature, T_M is the temperature at which $\alpha = 1$. Similarly, K at any temperature is calculated from the $\alpha(T)$ *versus* temperature curve. ΔH° and ΔS° are then determined from a $\ln(KT)$ *versus* $1/T$ plot for the slope and y intercept.

NMR spectroscopy

NMR experiments were acquired on either a Varian Inova 500 MHz or Varian Inova 800 MHz spectrometer with triple resonance and three axis gradient capabilities. NMR data were processed using either VNMR (Varian) or Felix (Molecular Simulations Incorporated, San Diego, CA) software. ^1H chemical shifts were referenced directly to trimethylsilylpropionic acid (TSP); ^{15}N and ^{13}C chemical shifts were referenced to known chemical shifts of imino nitrogen atoms and ribose carbon atoms in the UUCG tetraloop (Varani & Tinoco, 1991).

The exchangeable protons of the RNA were assigned using a combination of through-space homonuclear NOESY experiments at different temperatures (5, 15, and 25 °C) and different mixing times (75 ms, 150 ms, 250 ms), and through-bond correlation experiments of exchangeable protons and non-exchangeable protons in H_2O. Water suppression for these experiments was accomplished using either a 1:1 jump-return (Otting *et al*., 1987) or WATERGATE sequence (Piotto *et al*., 1992).

The non-exchangeable protons of the RNA were assigned with a combination of homonuclear NOESY experiments at different temperatures (15, 20, 25 and 35 °C) and different mixing times (50 ms, 100 ms, 150 ms, 250 ms and 300 ms), heteronuclear 3D (^{13}C) edited NOESY experiments (Clore *et al*., 1990) centered on either the aromatic or ribose portions of the carbon spectrum at 25 °C with a mixing time of 150 ms, and heteronuclear through-bond experiments. 3D HCCH-TOCSY (Clore *et al*., 1990; Nikonowicz & Pardi, 1992) was used to correlate protons within one spin system. 3D HCP (Marino *et al*., 1994b) and 2D $^1H/^{31}P$ heteronuclear COSY (Sklénar *et al*., 1986) were used to connect successive nucleotides through the ^{31}P. MQ-HCN (Marino *et al*., 1997) was used to correlate the H1′ and H8/H6. 2D HCCH-TOCSY (Marino *et al*., 1994a) was used to correlate the H2 and H8 resonances on the adenosine residues. The pyrimidine H5 and H6 were correlated by a DQF-COSY. Parameters for the DQF-COSY were 4096 complex points in ω2, 512 complex points in ω1, 4000 Hz sweep-width in both dimensions with 32 scans/increment and a relaxation delay of 1.5 seconds. Heteronuclear TOCSY experiments were used to correlate the water-exchangeable base protons with the non-exchangeable protons on the base (Simorre *et al*., 1995, 1996a,b).

Structure calculation

Structures were calculated on the RNA oligonucleotide using restrained molecular dynamics followed by energy minimization using the program X-PLOR on an SGI Octane workstation with a force-field consisting of bond lengths, bond angles, improper angles, repulsive van der Waals potentials, and experimental distance and dihedral constraints in the absence of electrostatics. Random starting structures were created by randomizing torsion angles for the calculation. The initial stage was a modified simulated annealing protocol (Wimberly *et al.*, 1993) that included experimental distance constraints but did not include dihedral constraints; structures that converged to low total energy were subjected to a refinement protocol that added in the experimental dihedral constraints. The structures were finally minimized with attractive Lennard-Jones potentials and electrostatics. The final structures were displayed with the program Insight II (Molecular Simulations Incorporated, San Diego, CA).

Distance restraints were assigned based upon NOE volumes of crosspeaks in NOESY experiments at short mixing time (50 ms), medium mixing time (100 ms), and long mixing time (150 ms). NOEs with volumes comparable to those of the H1′-H2′ and pyrimidine H5-H6 NOEs at short mixing time were assigned as strong and given a distance range of 1.8-3.0 Å. NOEs that were weaker than the strong NOEs at short mixing time but were intense at medium mixing time were assigned as medium and given a distance range of 2-4.5 Å. NOEs that were not intense until long mixing time were assigned as weak and given a distance range of 3-6 Å. NOEs that were weak in intensity at 150 ms were assigned as very weak and given a range of 3.5-7.5 Å. NOEs that were clearly identifiable but whose intensity was hard to define due to overlap were given wider ranges, reflective of what mixing time they were first observed. Water-exchangeable NOEs were assigned wide ranges based upon their intensity in a 75 ms mixing time NOESY in H_2O.

Dihedral constraints were determined from homonuclear and heteronuclear correlation experiments, except for the χ angle, which was assigned on the basis of the presence or absence of a strong H1′-H8/H6 NOE. All nucleotides were assigned as *anti*, except the G of the UUCG tetraloop as previously shown (Cheong *et al.*, 1990). *Anti* was assigned a range of −40°-180° (O4′-C1′-N9/N1-C4/C2) (Saenger, 1984).

The ribose sugar pucker was assigned on the basis of the size of the H1′-H2′ coupling constant determined in a DQF-COSY. A coupling constant >8 Hz was assigned as C2′-*endo*; a coupling constant <2 Hz was assigned as C3′-*endo*. Nucleotides with coupling constants between 2 Hz and 8 Hz were assigned as mixed and given a range of sugar puckers from C2′-*endo*, O4′-*endo* and C3′-*endo*. The values for each were from Saenger (1984).

The backbone torsion angles were essentially determined as described by Marino *et al.* (1999) and Fourmy *et al.* (1998). Overlap, particularly in phosphorus chemical shift prevented all angles from being identified. Values for these angles were from Saenger (1984) with ranges of ±20°. The backbone torsion angle ε was estimated from $^3J_{H3'\text{-}P}$, $^3J_{C2'\text{-}P}$, and $^3J_{C4'\text{-}P}$ from a 2D ^{31}P-^{1}H heteronuclear COSY (Sklénar *et al.*, 1986) and 3D HCP (Marino *et al.*, 1994b) and given a range of −155(±20)° except for c14 of the UUCG loop, which was given a range of −95(±20)°. The torsion angle β was estimated from $^3J_{H5'\text{-}P}$, $^3J_{H5''\text{-}P}$, and $^3J_{C4'\text{-}P}$ from the same experiments and given a range of 180(±20)°. The torsion angle β for G1408 and G1491-G1494 were not confidently assigned and not constrained. The torsion angle γ was estimated from $^3J_{H4'\text{-}H5'}$ from a ^{31}P decoupled DQF-COSY and a 3D ^{13}C-^{1}H HMQC-TOCSY, and given a range of 55(±20)° except for g15 of the UUCG loop that is *trans* and given a range of 180(±20). The torsion angle γ for G1408 and G1491-G1494 were not confidently assigned and not constrained.

Protein Data Bank accession code

The coordinates for the eukaryotic decoding-site oligonucleotide have been deposited in the RCSB protein data bank, accession number 1FYO.

Acknowledgments

We thank M. Recht, K. Dahlquist, R. G. Eason, S. Yoshizawa and S. Blanchard for many useful discussions on aminoglycosides and the ribosome, and P. Lukavsky for writing NMR pulse sequences used in these studies. This work was supported by NIH grant GM51266 and funding from Aventis Pharmaceuticals. The Stanford Magnetic Resonance Laboratory is supported by the Stanford School of Medicine.

References

Cate, J. H., Yusupov, M. M., Yusupova, G. Z., Earnest, T. N. & Noller, H. F. (1999). X-ray crystal structures of 70 S ribosome functional complexes. *Science,* **285**, 2095-2104.

Cheong, C., Varani, G. & Tinoco, I., Jr (1990). Solution structure of an unusually stable RNA hairpin, 5′GGAC(UUCG)GUCC. *Nature,* **346**, 680-682.

Clemons, W. M., May, J. L., Wimberly, B. T., McCutcheon, J. P., Capel, M. S. & Ramakrishnan, V. (1999). Structure of a bacterial 30 S ribosomal subunit at 5.5 Å resolution. *Nature,* **400**, 833-840.

Clore, G. M., Bax, A., Driscoll, P. C., Wingfield, P. T. & Gronenborn, A. M. (1990). Assignment of the side-chain ^{1}H and ^{13}C resonances of Interleukin-1β using double- and triple-resonance heteronuclear three-dimensional NMR spectroscopy. *Biochemistry,* **29**, 8172-8184.

Dahlquist, K. D. & Puglisi, J. D. (2000). Interaction of translation initiation factor IF1 with the *E. coli* ribosomal A site. *J. Mol. Biol.* **299**, 1-15.

Davies, J., Gorini, L. & Davis, B. D. (1965). Misreading of RNA codewords induced by aminoglycoside antibiotics. *Mol. Pharmacol.* **1**, 93-106.

Edelmann, P. & Gallant, J. (1977). Mistranslation in *E. coli*. *Cell,* **10**, 131-137.

Fourmy, D., Recht, M. I., Blanchard, S. C. & Puglisi, J. D. (1996). Structure of the A site of *E. coli* 16 S ribosomal RNA complexed with an aminoglycoside antibiotic. *Science,* **274**, 1367-1371.

Fourmy, D., Yoshizawa, S. & Puglisi, J. D. (1998). Paromomycin binding induces a local conformational change in the A site of 16 S rRNA. *J. Mol. Biol.* **277**, 333-345.

Gutell, R. R. (1994). Collection of small subunit (16 S and 16 S-like) ribosomal RNA structures: 1994. *Nucl. Acids Res.* **22**, 3502-3507.

Lodmell, J. S. & Dahlberg, A. E. (1997). A conformational switch in *Escherichia coli* 16 S ribosomal RNA during decoding of messenger RNA. *Science,* **277**, 1262-1267.

Lynch, S. R. & Puglisi, J. D. (2001). Structural origins of aminoglycoside specificity for prokaryotic ribosomes. *J. Mol. Biol.* **306**, 1037-1058.

Marino, J. P., Prestegard, J. H. & Crothers, D. M. (1994a). Correlation of adenine H2/H8 resonances in uniformly ^{13}C labeled RNAs by 2D HCCH-TOCSY: a new tool for ^{1}H assignment. *J. Am. Chem. Soc.* **116**, 2205-2206.

Marino, J. P., Schwalbe, H., Anklin, C., Bermel, W., Crothers, D. M. & Griesinger, C. (1994b). A three-dimensional triple-resonance ^{1}H, ^{13}C, ^{31}P experiment: sequential through-bond correlation of ribose protons and intervening phosphorus along the RNA oligonucleotide backbone. *J. Am. Chem. Soc.* **116**, 6472-6473.

Marino, J. P., Diener, J. L., Moore, P. B. & Griesinger, C. (1997). Multiple-quantum coherence dramatically enhances the sensitivity of CH and CH_2 correlations in uniformly ^{13}C-labeled RNA. *J. Am. Chem. Soc.* **119**, 7361-7366.

Marino, J. P., Schwalbe, H. & Griesinger, C. (1999). J-coupling restraints in RNA structure determination. *Accts. Chem. Res.* **32**, 614-623.

Marky, L. A. & Breslauer, K. J. (1987). Calculating thermodynamic data for transitions of any molecularity from equilibrium melting curves. *Biopolymers,* **26**, 1601-1620.

Moazed, D. & Noller, H. F. (1986). Transfer RNA shields specific nucleotides in 16 S ribosomal RNA from attack by chemical probes. *Cell,* **47**, 985-994.

Moazed, D. & Noller, H. F. (1987). Interaction of antibiotics with functional sites in 16 S ribosomal RNA. *Nature,* **327**, 389-394.

Moazed, D., Samaha, R. R., Gualerzi, C. & Noller, H. F. (1995). Specific protection of 16 S rRNA by translational initiation factors. *J. Mol. Biol.* **248**, 207-210.

Nikonowicz, E. P. & Pardi, A. (1992). Three-dimensional heteronuclear NMR studies of RNA. *Nature,* **355**, 184-186.

Noller, H. F. (1991). Ribosomal RNA and translation. *Annu. Rev. Biochem.* **60**, 191-227.

Otting, G., Grutter, R., Leupin, W., Minganti, C., Ganesh, K. N., Sproat, B. S., Gait, M. J. & Wuthrich, K. (1987). Sequential NMR assignments of labile protons in DNA using two-dimensional nuclear-Overhauser-enhancement spectroscopy with three jump-and-return pulse sequences. *Eur. J. Biochem.* **166**, 215-220.

Piotto, M., Saudek, V. & Sklenár, V. (1992). Gradient-tailored excitation for single-quantum NMR spectroscopy of aqueous solutions. *J. Biomol. NMR,* **2**, 661-665.

Puglisi, J. D. & Wyatt, J. R. (1995). Biochemical and NMR studies of RNA conformation with an emphasis on RNA pseudoknots. *Methods Enzymol.* **261**, 323-350.

Recht, M. I., Fourmy, D., Blanchard, S. C., Dahlquist, K. D. & Puglisi, J. D. (1996). RNA sequence determinants for aminoglycoside binding to an A-site rRNA model oligonucleotide. *J. Mol. Biol.* **262**, 421-436.

Recht, M. I., Douthwaite, S. & Puglisi, J. D. (1999). Basis for prokaryotic specificity of action of aminoglycoside antibiotics. *EMBO J.* **18**, 3133-3138.

Saenger, W. (1984). *Principles of Nucleic Acid Structure*, Springer-Verlag, Berlin.

Simorre, J.-P., Zimmermann, G. R., Pardi, A., Farmer, B. T. I. & Mueller, L. (1995). Triple resonance HNCCCH experiments for correlating exchangeable cytidine and uridine base protons in RNA. *J. Biomol. NMR,* **6**, 427-432.

Simorre, J.-P., Zimmermann, G. R., Mueller, L. & Pardi, A. (1996a). Correlations of the guanosine exchangeable and nonexchangeable base protons in ^{13}C-^{15}N-labeled RNA with an HNC-TOCSY-CH experiment. *J. Biomol. NMR,* **7**, 153-156.

Simorre, J. P., Zimmermann, G. R., Mueller, L. & Pardi, A. (1996b). Triple-resonance experiments for assignment of adenine base resonances in $^{13}C/^{15}N$ labeled RNA. *J. Am. Chem. Soc.* **118**, 5316-5317.

Sklénar, V., Miyashiro, H., Zon, G. & Bax, A. (1986). Assignment of the ^{31}P and ^{1}H resonances in oligonucleotides by two-dimensional NMR spectroscopy. *FEBS Letters,* **208**, 94-98.

Varani, G. & Tinoco, I., Jr (1991). Carbon assignments and heteronuclear coupling constants for an RNA oligonucleotide form natural abundance ^{13}C-^{1}H correlated experiments. *J. Am. Chem. Soc.* **113**, 9349-9354.

Varani, G., Cheong, C. & Tinoco, I., Jr (1991). Structure of an unusually stable RNA hairpin. *Biochemistry,* **30**, 3280-3289.

Wimberly, B., Varani, G. & Tinoco, I., Jr (1993). The conformation of loop E of eukaryotic 5 S ribosomal RNA. *Biochemistry,* **32**, 1078-1087.

Woodcock, J., Moazed, D., Cannon, M., Davies, J. & Noller, H. F. (1991). Interaction of antibiotics with A- and P-site-specific bases in 16 S ribosomal RNA. *EMBO J.* **10**, 3099-3103.

Yoshizawa, S., Fourmy, D. & Puglisi, J. D. (1998). Structural origins of gentamicin antibiotic action. *EMBO J.* **17**, 6437-6448.

Yoshizawa, S., Fourmy, D. & Puglisi, J. D. (1999). Recognition of the codon-anticodon helix by ribosomal RNA. *Science,* **285**, 1722-1725.

Edited by I. Tinoco

(Received 11 July 2000; received in revised form 10 October 2000; accepted 20 December 2000)